

# FLEXIBLE 3D CAGE-BASED DEFORMATION VIA GREEN COORDINATES ON BÉZIER PATCHES

A PREPRINT

 **Dong Xiao**

School of Mathematical Sciences  
University of Science and Technology of China  
xiaodong@ustc.edu.cn

 **Renjie Chen\***

School of Mathematical Sciences  
University of Science and Technology of China  
renjiechen@ustc.edu.cn

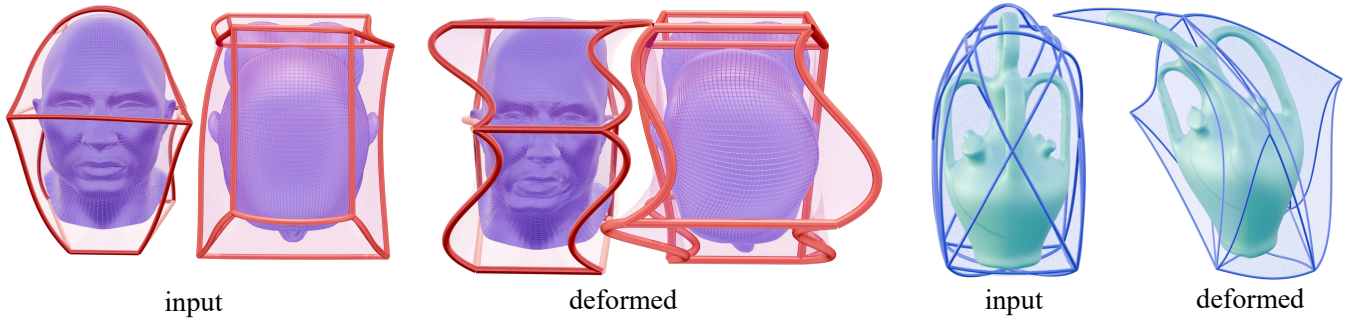


Figure 1: The high-order structure of Bézier patches (left: tensor product Bézier patches, right: Bézier triangles) allows us to design a tightly fitted cage and achieve curved deformations.

## ABSTRACT

Cage-based deformation is a fundamental problem in geometry processing, where a cage, a user-specified boundary of a region, is used to deform the ambient space of a given mesh. Traditional 3D cages are typically composed of triangles and quads. While quads can represent non-planar regions when their four corners are not coplanar, they form ruled surfaces with isoparametric curves being line segments, which limits their ability to handle curved and high-curvature deformations. In this work, we extend the cage for curved boundaries using Bézier patches, enabling flexible and high-curvature deformations with only a few control points. The higher-order structure of the Bézier patch also allows for the creation of a more compact and precise curved cage for the input model. Based on Green’s third identity, we derive the Green coordinates for the Bézier cage, achieving shape preserving deformation with smooth surface boundaries. These coordinates are defined based on the vertex positions and normals of the Bézier control net. Given that the coordinates are approximately calculated through Riemann summation, we propose a global projection technique to ensure that the coordinates accurately conform to the linear reproduction property. Experimental results show that our method achieves high performs in handling curved and high-curvature deformations.

**Keywords** Cage-based deformation · Green coordinates · Bézier surface · Linear reproduction

## 1 Introduction

Space deformation is a widely studied topic in geometry processing, primarily focused on deforming the ambient space of an embedded shape [Ben-Chen et al., 2009]. One commonly used method is cage-based deformation, where the embedded space deforms according to the changes in the cage as the user manipulates the shape from the source cage to the target cage.

Cage-based deformation primarily constructs barycentric coordinates, which form a partition of unity  $\phi_i(\eta)$  for each point  $\eta \in \mathbb{R}^3$  within the cage, satisfying  $\sum_{i=1}^N \phi_i(\eta) = 1$  and  $\eta = \sum_{i=1}^N \phi_i(\eta) \mathbf{v}_i$ , where  $\mathbf{v}_i$  represent the cage vertices. Various methods exist for computing these coordinates, such as Mean Value Coordinates [Ju et al., 2005, Thiery et al., 2018], Harmonic Coordinates [Joshi et al., 2007], and Poisson Co-

ordinates [Li and Hu, 2013]. However, these methods do not prioritize the conformal property, which may result in shearing artifacts. To address this issue, Lipman et al. [2008] introduce Green coordinates, which take into account both the cage vertices and the cage normals. Green coordinates are expressed as  $\eta = \sum_{i=1}^N \phi_i(\eta) \mathbf{v}_i + \sum_{j=1}^M \psi_j(\eta) \mathbf{n}_j$ , achieving quasi-conformal mapping in 3D and exhibiting shape preserving effects.

Besides coordinates, another key factor is the geometry of the cage structure. Earlier work always represent the cage as an oriented simplicial surface [Ju et al., 2005, Lipman et al., 2008, Ben-Chen et al., 2009], which preforms limited capabilities for shape control. To fill this gap, Thiery et al. [2018] and Thiery and Boubekur [2022] propose mean value coordinates and Green coordinates for tri-quad cages. A quadrilateral (quad) in 3D can represent a non-planar region when its four vertices are not co-planar. However, every isoparametric curve of the quad is straight, making it challenging to control curved deformations. To adapt to high curvature deformations, Michel and Thiery [2023] propose polynomial cages and achieve flexible deformations for curved shapes. However, this method is only available in 2D. Moreover, S-patch [Smith and Schaefer, 2015] and  $C^0$  GC patch [Qin et al., 2024] can be utilized to construct barycentric coordinates for high-order structures in 3D. However, it is non-trivial for them to establish Green coordinates with shape-preserving capabilities due to the absence of cage normals.

In this research, we utilize Bézier patches to represent 3D cages and construct Green coordinates for cage-based deformation. To the best of our knowledge, this is the first work to construct coordinates with normal control for high-order cages with curved boundaries in 3D. The flexibility of our approach is demonstrated in the following two aspects: 1) The curved structure of Bézier patches enables us to design a more compact and tightly fitted cage for the input model; and 2) The smoothness of Bézier patches enables a more flexible 3D shape deformation, particularly for curved and high-curvature scenarios.

We derive the Green coordinates for the Bézier cage based on Green’s third identity, which facilitate a shape-preserving deformation. Given that establishing Green coordinates requires cage normals, our method construct surface normals based on the Bézier control net and subsequently express the coordinates in terms of both the positions and normals of the control vertices. Due to the absence of a closed-form solution for the integration, we utilize Riemann summation to approximately calculate the coordinates. We then introduce a global projection method to map these approximate results onto the solution space that satisfies precise linear reproduction, ensuring the theoretical validity of the results.

Fig. 1 shows typical examples of our approach, in which we design tightly fitted Bézier cages (left: tensor product Bézier patches, right: Bézier triangles) to achieve curved deformation. In the experimental section, we compare our method with other coordinate systems and cage representations. The results demonstrate that our approach yields smooth surface boundaries by leveraging higher-order structures and achieves

superior performance in handling curved and high-curvature deformations.

## 2 Related work

Cage-based deformation has received considerable attention due to its broad range of applications. Given a cage, various methods can be employed to establish the coordinates, depending on the type of cage and the specific geometric requirements. In this section, we will introduce the most relevant work to our study. For a comprehensive review of different coordinate systems, one can refer to [Floater, 2015] and [Hormann and Sukumar, 2017]. Additionally, Ströter et al. [2024] provide a comprehensive survey for cage-based deformation in 3D environments.

**Interpolatory coordinates.** Interpolatory coordinates mainly represent the position within a geometric shape by a set of weights that form a partition of unity. Most of these coordinates are known as Generalized Barycentric Coordinates (GBC), which are extensively discussed in [Hormann and Sukumar, 2017]. These coordinates are widely utilized in cage-based deformation [Yan and Schaefer, 2019, Dodik et al., 2023]. Mean Value Coordinates (MVC), initially proposed for 2D [Floater, 2003] and 3D [Floater et al., 2005] polygons, have inspired numerous subsequent studies. Ju et al. [2005] define MVC for 3D triangle meshes and utilize this technique for cage-based deformation by projecting the cage onto a unit sphere. Building on a similar concept, Langer et al. [2006] propose spherical barycentric coordinates for planar n-gons; Lipman et al. [2007] introduce Positive Mean Value Coordinates (PMVC), which eliminate artifacts for non-convex cages by addressing the negative weights generated by the original MVC. Li and Hu [2013] introduce Poisson coordinates based on the Poisson integral formula, which can be considered an extension of the MVC framework. Furthermore, several studies extend MVC to higher-order cages. Cubic Mean Value coordinates [Li et al., 2013] enable the handling of curved cages with cubic boundaries. QMVC [Thiery et al., 2018] constructs MVC for tri-quad cages, extending this technique to non-planar 3D quads.

Besides the MVC framework, other techniques have also been widely explored. Joshi et al. [2007] construct Harmonic coordinates by numerically solving the Laplace equation. Maximum Entropy Coordinates Hormann and Sukumar [2008] and Maximum Likelihood Coordinates Chang et al. [2023] conceptualize coordinates as probability distributions and construct the coordinate system using probability theory.

**Coordinates with normal control.** In addition to barycentric coordinates, another important class is known as Green coordinates [Lipman et al., 2008], which consider not only the vertices but also the normals. Green coordinates have a closed-form solution for triangle meshes, which is thoroughly derived in Lipman and Levin [2009]. Many works establish Green coordinates on different cage structures. Michel and Thiery [2023] and Liu et al. [2024a] proposes polynomial 2D Green coordinates and derive closed-form solutions. Thiery and Boubekur [2022] extend Green coordinates to tri-quad cages

in 3D and employ robust Riemann summation for coordinate computation.

There are also other normal controlled coordinate systems, such as biharmonic coordinates Weber et al. [2012], Thiery et al. [2024] and Somigliana coordinates Chen et al. [2023]. Additionally, Cauchy coordinates Weber et al. [2009] and polynomial Cauchy coordinates Lin and Chen [2024], which are constructed in the complex plane, can be regarded as equivalent to Green coordinates after specific derivations. To the best of our knowledge, there are currently no Green coordinates defined on high-order cages with curved boundaries in a 3D scenario.

**High order structures.** Previous works on geometric modeling typically utilized piecewise linear data to represent various shapes. However, in recent years, there has been a growing emphasis on high-order structures, including Bézier triangles, Bézier tetrahedrals, and tensor product Bézier surfaces Farin [1992a]. Researchers such as Hu et al. [2019], Mandad and Campen [2020], and Yang et al. [2022] employ diverse strategies to construct high-order meshing in 2D domains. Jiang et al. [2021] proposes an automatic algorithm to convert 3D triangle meshes to high-order meshes. Liu et al. [2024b] develop a new strategy to construct high-order shells from input meshes and facilitate attribute transfer between the two shells.

In addition, several studies explore the application of high-order concepts to shape deformation. For instance, Smith and Schaefer [2015] and Qin et al. [2024] propose generalized barycentric coordinates using transfinite interpolation techniques, which can be extended to cage-based deformation. However, these methods usually lack normal controls, which poses challenges for achieving shape-preserving deformations.

### 3 Preliminaries

#### 3.1 Green coordinates for cage-based deformation

Cage-based deformation with normal control can yield more realistic and shape preserving results. We will first recall the Green coordinates for oriented simplicial surfaces Lipman et al. [2008]. The source cage is represented as a triangle mesh with vertices  $\{\mathbf{v}_i\}_{i=1}^N$ , faces  $\{f_j\}_{j=1}^M$  and face normals  $\{\mathbf{n}_j\}_{j=1}^M$ , where  $N$  and  $M$  represent the number of vertices and faces. Green coordinates primarily construct a series of functions  $\{\phi_i(\eta)\}_{i=1}^N$  and  $\{\psi_j(\eta)\}_{j=1}^M$  regarding the cage vertices and normals to describe an arbitrary position  $\eta$  within the cage, which can be expressed as:

$$\eta = \sum_{i=1}^N \phi_i(\eta) \mathbf{v}_i + \sum_{j=1}^M \psi_j(\eta) \mathbf{n}_j. \quad (1)$$

Then, we can modify the original shape according to our requirements. If the vertices and normals of the target cage are  $\{\tilde{\mathbf{v}}_i\}_{i=1}^N$  and  $\{\tilde{\mathbf{n}}_i\}_{i=1}^M$ , respectively, the deformed location  $\tilde{\eta}$  is calculated as:

$$\tilde{\eta} = \sum_{i=1}^N \phi_i(\eta) \tilde{\mathbf{v}}_i + \sum_{j=1}^M \psi_j(\eta) s_j \tilde{\mathbf{n}}_j, \quad (2)$$

where  $s_j$  is a scalar factor to maintain quasi-conformality, whose computation method is detailed in Lipman et al. [2008] and Thiery and Boubekeur [2022].

The construction of Green coordinates (*i.e.*, the calculation of  $\phi_i(\eta)$  and  $\psi_j(\eta)$  in Eq. (1)) is mainly based on the Green's third identity. If  $\Omega$  is a bounded region in  $\mathbb{R}^3$  and function  $f$  is harmonic. Then, for arbitrary  $\eta \in \Omega$ ,  $f(\eta)$  can be expressed as a boundary integration:

$$f(\eta) = \underbrace{\int_{\xi \in \partial\Omega} f(\xi) \frac{\partial G}{\partial n}(\xi, \eta) d\xi}_{f_D(\eta)} - \underbrace{\int_{\xi \in \partial\Omega} G(\xi, \eta) \frac{\partial f}{\partial n}(\xi) d\xi}_{f_N(\eta)}, \quad (3)$$

where  $G$  is the fundamental solutions of the Laplace equation  $\Delta G_\xi(\xi, \eta) = \delta(\|\xi - \eta\|)$ . In 3D,  $G$  has the following expression:

$$G(\xi, \eta) = -\frac{1}{4\pi\|\xi - \eta\|}. \quad (4)$$

The directional derivative of  $G$  with respect to  $\xi$  can be expressed as:

$$\frac{\partial G}{\partial n}(\xi, \eta) = \frac{(\xi - \eta) \cdot \mathbf{n}_\xi}{4\pi\|\xi - \eta\|^3}, \quad (5)$$

where  $\mathbf{n}_\xi$  is the normal at  $\xi$ .

Eq. (3) gives a continuous representation of  $f$  as a boundary integral. When the cage is a triangle mesh, we want  $f$  to be piecewise linear on the cage. Lipman et al. [2008] propose the following expression for  $f$ :

$$f(\xi) = \sum_{i \in N_{gbr}(\xi)} \Gamma^i(\xi) \mathbf{v}_i, \quad (6)$$

where  $\Gamma^i(\xi)$  is a hat function that takes the value 1 at  $\mathbf{v}_i$ , 0 at all other vertices, and varies linearly across each face of its 1-ring neighbour. Then, the coordinates  $\phi_i(\eta)$  and  $\psi_j(\eta)$  can be calculated as:

$$\begin{aligned} \phi_i(\eta) &= \int_{\xi \in F_1(i)} \Gamma^i(\xi) \frac{\partial G}{\partial n}(\xi, \eta) d\xi, \\ \psi_j(\eta) &= \int_{\xi \in t_j} -G(\xi, \eta) d\xi, \end{aligned} \quad (7)$$

where  $F_1(i)$  denotes the 1-ring neighbour of  $\mathbf{v}_i$ .

While Lipman et al. [2008] originally define Green coordinates on triangle meshes, Thiery and Boubekeur [2022] extend this technique to quad meshes. A quad  $\mathbf{q}(u, v)$  is represented as a bilinear interpolation surface of four vertices  $\{\mathbf{q}_i\}_{i=0}^3$ , governed by following parameterization equation:

$$\mathbf{q}(u, v) = (1-u)(1-v)\mathbf{q}_0 + u(1-v)\mathbf{q}_1 + uv\mathbf{q}_2 + v(1-u)\mathbf{q}_3. \quad (8)$$

A quad can define a non-planar ruled surface, where every isoparametric curve  $\mathbf{q}(u_0, v)$  and  $\mathbf{q}(u, v_0)$  is straight. Inspired by polynomial Green coordinates proposed by Michel and Thiery [2023] in 2D, which construct the cage with polynomial curves as  $f(t) = \sum_i c_i t^i$ , we propose to extend the 3D cage with higher-order structures.

### 3.2 Tensor product Bézier surfaces

Triangle meshes are limited to first-order approximations due to their piecewise linearity, which restricts their ability to accurately represent continuous surfaces. To address this limitation, previous studies have explored the use of high-order geometric representations to enhance surface expression. A Bézier patch is typically constructed as a high-order parametric surface from a series of control points. Our method is capable of handling various cage types including both tensor product Bézier surfaces and Bézier triangles. In the main text, we primarily focus on tensor product Bézier surfaces for illustrative purposes, while detailed discussions on Bézier triangles are presented in Appendix A of the supplementary material.

A tensor product Bézier patch is governed by two parameters  $u$  and  $v$ , constrained by  $0 \leq u \leq 1, 0 \leq v \leq 1$ . which can be understood as moving a Bézier curve along another Bézier curve. A degree- $(m, n)$  Bézier patch  $\mathbf{b}(u, v)$  has  $(m+1) \times (n+1)$  control points  $\mathbf{b}_{ij}, i \in \{0, 1, 2, \dots, m\}, j \in \{0, 1, 2, \dots, n\}$ . The expression for the Bézier patch is given by:

$$\mathbf{b}(u, v) = \sum_{i=0}^m \sum_{j=0}^n \frac{m!}{i!(m-i)!} \frac{n!}{j!(n-j)!} u^i (1-u)^{m-i} v^j (1-v)^{n-j} \mathbf{b}_{ij}. \quad (9)$$

We can denote  $\lambda^{ij}(u, v) = B_i^m(u)B_j^n(v) = \frac{m!}{i!(m-i)!} \frac{n!}{j!(n-j)!} u^i (1-u)^{m-i} v^j (1-v)^{n-j}$ , which is the product of two Bernstein polynomials. Consequently, we have:

$$\mathbf{b}(u, v) = \sum_{i=0}^m \sum_{j=0}^n \lambda^{ij}(u, v) \mathbf{b}_{ij}. \quad (10)$$

## 4 Method

### 4.1 Green coordinates for Bézier cage

In this section, we derive the Green's coordinates for the Bézier cage composed of tensor product Bézier patches as defined by Eq. (10). Our cage ensures no self-intersection throughout its entire structure. A key observation is that, although the parameters  $u$  and  $v$  are of high degree, the function  $\mathbf{b}(u, v)$  is linear with respect to the positions of control points  $\mathbf{b}_{ij}$ . Consequently, we can expect to establish Green coordinates in relation to the Bézier control net. However, normals are also necessary for constructing the coordinates. For triangle meshes, planar face normals can be directly calculated and applied. However, for high-order Bézier patches, the (unnormalized) normal is expressed as  $(\mathbf{b}_u \times \mathbf{b}_v)(u, v)$ , which is non-trivial to represent directly using the normals of the control net. Nevertheless, some studies propose approximating the normal of a Bézier patch by interpolating the normals of the control vertices and substituting these normals into the parametric formulation [Vlachos et al., 2001, Owen et al., 2002]. This inspires us to apply a similar approach to approximate unnormalized normals  $(\mathbf{b}_u \times \mathbf{b}_v)(u, v)$  for the tensor product Bézier patch. In the subsequent derivations and following sections, we

will frequently require unnormalized normals, and we will no longer explicitly refer to the term ‘‘unnormalized’’.

Given a degree- $(m, n)$  tensor product Bézier patch with control net  $\mathbf{b}_{ij}$ , where  $i \in \{0, 1, 2, \dots, m\}, j \in \{0, 1, 2, \dots, n\}$ , we first compute the normals  $\mathbf{N}_{ij}$  for each vertex  $\mathbf{b}_{ij}$ . We first take the normal  $\mathbf{N}_{00}$  at a corner in Fig. 2 (b) as an example. The control net is piecewise linear at the quad  $(\mathbf{b}_{00}, \mathbf{b}_{10}, \mathbf{b}_{11}, \mathbf{b}_{01})$ , which has following parametric equation:

$$\mathbf{q}^{00}(u, v) = (1-mu)(1-nv)\mathbf{b}_{00} + mu(1-nv)\mathbf{b}_{10} + mn \cdot uv\mathbf{b}_{11} + nv(1-mu)\mathbf{b}_{01}, u \in [0, \frac{1}{m}], v \in [0, \frac{1}{n}]. \quad (11)$$

Therefore,  $\mathbf{N}_{00}$  can be calculated as:

$$\mathbf{N}_{00} = (\mathbf{q}_u^{00} \times \mathbf{q}_v^{00})|_{\{u=v=0\}} = mn[(\mathbf{b}_{10} - \mathbf{b}_{00}) \times (\mathbf{b}_{01} - \mathbf{b}_{00})]. \quad (12)$$

For the interior control point  $\mathbf{b}_{ij}$ , its normal  $\mathbf{N}_{ij}$  can be calculated by the average of its 1-ring neighbour at the control net using the following formulation:

$$\mathbf{N}_{ij} = \frac{mn}{4} [(\mathbf{b}_{i(j+1)} - \mathbf{b}_{ij}) \times (\mathbf{b}_{(i-1)j} - \mathbf{b}_{ij}) + (\mathbf{b}_{(i-1)j} - \mathbf{b}_{ij}) \times (\mathbf{b}_{i(j-1)} - \mathbf{b}_{ij}) + (\mathbf{b}_{i(j-1)} - \mathbf{b}_{ij}) \times (\mathbf{b}_{(i+1)j} - \mathbf{b}_{ij}) + (\mathbf{b}_{(i+1)j} - \mathbf{b}_{ij}) \times (\mathbf{b}_{i(j+1)} - \mathbf{b}_{ij})]. \quad (13)$$

After determining the normals of the control vertices, we can approximate the surface normal  $\mathbf{N}(u, v)$  for arbitrary  $(u, v)$  of the Bézier patch using the following expression:

$$\mathbf{N}(u, v) = \sum_{i=0}^m \sum_{j=0}^n \lambda^{ij}(u, v) \mathbf{N}_{ij}, \quad (14)$$

$\lambda^{ij}(u, v)$  is the Bernstein basis function of the Bézier patch, which is identical to Eq. (10).  $\mathbf{N}(u, v)$  approximates  $(\mathbf{b}_u \times \mathbf{b}_v)(u, v)$  and is linear with respect to the normals  $\mathbf{N}_{ij}$  of the control vertices. This linearity facilitates the derivation of the Neumann term in Green coordinates.

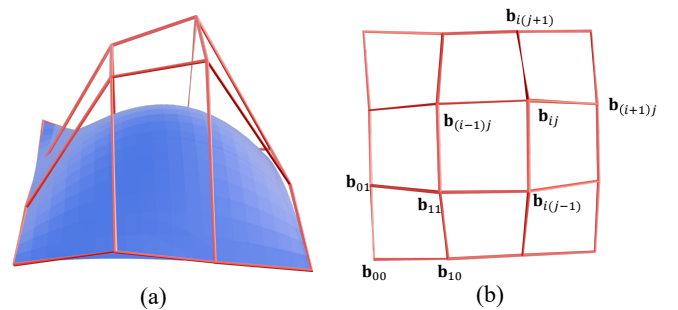


Figure 2: Illustration of a tensor product Bézier patch (a) and its control net (b).

The coordinates is constructed based on the Green's third identity (Eq. (3)). We represent the Dirichlet term as  $f_D(\eta)$  and Neumann term as  $f_N(\eta)$ , where  $f(\eta) = f_D(\eta) + f_N(\eta)$ . Let  $f(\eta) = \eta$ , then  $f$  is harmonic, and we obtain a continuous

representation of  $\eta$  as a boundary integral. Here, we directly derive the deformed position  $\tilde{\eta}$  within a continuous formulation. In the following, we will denote the values after deformation with tilde lines (e.g.,  $\tilde{\mathbf{b}}(u, v)$ ,  $\tilde{f}_D^Q(\eta)$ ,  $\tilde{\eta}$ ), while those before deformation remain without tilde lines (e.g.,  $\mathbf{b}(u, v)$ ,  $\mathbf{b}_u(u, v)$ ,  $\eta$ ). The Dirichlet term  $\tilde{f}_D^Q(\eta)$  and Neumann term  $\tilde{f}_N^Q(\eta)$  of one Bézier patch  $Q$  can be expressed as follows:

$$\tilde{f}_D^Q(\eta) = \int_{\xi \in Q} \tilde{f}(\xi) \frac{\partial G}{\partial n}(\xi, \eta) d\xi, \quad (15)$$

where

$$\tilde{f}(\xi) = \tilde{\mathbf{b}}(u, v), \quad (16)$$

$$\frac{\partial G}{\partial n}(\xi, \eta) = \frac{\mathbf{b}(u, v) - \eta}{4\pi \|\mathbf{b}(u, v) - \eta\|^3} \cdot \frac{\mathbf{b}_u(u, v) \times \mathbf{b}_v(u, v)}{\|\mathbf{b}_u(u, v) \times \mathbf{b}_v(u, v)\|}, \quad (17)$$

$$d\xi = \|\mathbf{b}_u(u, v) \times \mathbf{b}_v(u, v)\| dvdu. \quad (18)$$

Additionally,

$$\tilde{f}_N^Q(\eta) = - \int_{\xi \in Q} G(\xi, \eta) \frac{\partial \tilde{f}}{\partial n}(\xi) s(\xi) d\xi, \quad (19)$$

where

$$G(\xi, \eta) = - \frac{1}{4\pi \|\mathbf{b}(u, v) - \eta\|}, \quad (20)$$

$$\frac{\partial \tilde{f}}{\partial n}(\xi) = \frac{\tilde{\mathbf{b}}_u(u, v) \times \tilde{\mathbf{b}}_v(u, v)}{\|\tilde{\mathbf{b}}_u(u, v) \times \tilde{\mathbf{b}}_v(u, v)\|}, \quad (21)$$

$$s(\xi) = \frac{\|\tilde{\mathbf{b}}_u(u, v) \times \tilde{\mathbf{b}}_v(u, v)\|}{\|\mathbf{b}_u(u, v) \times \mathbf{b}_v(u, v)\|}, \quad (22)$$

$$d\xi = \|\mathbf{b}_u(u, v) \times \mathbf{b}_v(u, v)\| dvdu. \quad (23)$$

In Eq. (19),  $s(\xi)$  serves as a scale factor to ensure quasi-conformality, and it can be set to the ratio of the surface element size after deformation to its size before deformation Thiery and Boubekeur [2022]. We substitute the expressions for each part into Eq. (15) and (19), and replace  $\tilde{\mathbf{b}}(u, v)$  with the parametric equation (10). When calculating the Neumann term, we approximate the cross product ( $\tilde{\mathbf{b}}_u(u, v) \times \tilde{\mathbf{b}}_v(u, v)$ ) as  $\tilde{\mathbf{N}}(u, v)$  from Eq. (14). After rearranging the formulas, the deformed position  $\tilde{\eta}$  can be computed as:

$$\tilde{\eta} = \sum_Q (\tilde{f}_D^Q(\eta) + \tilde{f}_N^Q(\eta)) = \sum_Q \sum_{i=0}^m \sum_{j=0}^n (\phi_Q^{ij}(\eta) \tilde{\mathbf{b}}_{ij}^Q + \psi_Q^{ij}(\eta) \tilde{\mathbf{N}}_{ij}^Q), \quad (24)$$

where

$$\phi_Q^{ij}(\eta) = \iint_{u,v=0}^1 \frac{\lambda_Q^{ij}(u, v) (\mathbf{b}_Q(u, v) - \eta) \cdot \mathbf{N}_Q(u, v)}{4\pi \|\mathbf{b}_Q(u, v) - \eta\|^3} dvdu, \quad (25)$$

$$\psi_Q^{ij}(\eta) = \iint_{u,v=0}^1 \frac{\lambda_Q^{ij}(u, v)}{4\pi \|\mathbf{b}_Q(u, v) - \eta\|} dvdu. \quad (26)$$

In above equations,  $Q$  represent a single patch of the Bézier cage,  $\tilde{\mathbf{b}}_{ij}^Q$  and  $\tilde{\mathbf{N}}_{ij}^Q$  denote the positions and normals of the control net of  $Q$  in the deformed cage.  $\mathbf{b}_Q(u, v)$  is the parametric

equation of the source cage,  $\lambda_Q^{ij}(u, v)$  represents the Bernstein parameter for the point  $\mathbf{b}_{ij}^Q$ , and  $\mathbf{N}_Q(u, v)$  denotes the normal of the source cage. This normal will be incorporated into the solid angle calculation in a subsequent step.

## 4.2 Approximated calculations for $\phi$ and $\psi$

In polynomial 2D Green coordinates Michel and Thiery [2023], Liu et al. [2024a], a closed-form expression can be derived because the integration involves a rational function of a single variable. However, in the 3D case, the denominators of  $\phi$  (Eq. (25)) and  $\psi$  (Eq. (26)) are polynomials of degree 3/2 and 1/2 in two variables  $u$  and  $v$ . Consequently, to the best of our knowledge, obtaining a closed-form solution is challenging. Inspired by the Riemann summation approach proposed by Thiery and Boubekeur [2022], we discretize the integral region  $u \in [0, 1]$ ,  $v \in [0, 1]$  of the Bézier patch  $Q$  into smaller triangle elements  $t$  and approximate the coordinates using Riemann summation. Although this approximation introduces some degree of error (typically the error remains relatively small), we have developed techniques to achieve precise linear reproduction, which will be elaborated upon in Section 4.3.

The denominator of  $\phi$  is a cubic function of  $(\mathbf{b}_Q(u, v) - \eta)$ , which suggests that we need to make finer divisions in areas closer to  $\eta$  to achieve more accurate calculations. Therefore, we first project  $\eta$  onto the Bézier patch  $Q$  and obtain the parameter of the closest point  $(u_Q, v_Q)(\eta)$ . This constitutes a point inversion problem Hu and Wallner [2005], and we employ gradient descent method to optimize the point-to-surface distance. Subsequently, we employ a UV pattern proposed by Thiery and Boubekeur [2022] to tessellate the parameter space  $[0, 1] \times [0, 1]$ , ensuring dense subdivision in regions closer to  $\eta$ . After decomposing the integration domain into small triangles (denotes as  $t$ ), the coordinates of the Dirichlet term  $\phi_Q^{ij}(\eta)$  of Eq. (25) can be approximated calculated as:

$$\begin{aligned} \phi_Q^{ij}(\eta) &= \sum_t \iint_{(u,v) \in t} \frac{\lambda_t^{ij}(u, v)}{4\pi} \frac{\overbrace{(\mathbf{b}_t(u, v) - \eta) \cdot \mathbf{N}_t(u, v)}^{\omega_t(\eta)}}{\|\mathbf{b}_t(u, v) - \eta\|^3} dvdu \\ &\approx \sum_t \frac{\lambda_t^{ij}(u_t, v_t)}{4\pi} \omega_t(\eta), \end{aligned} \quad (27)$$

where  $\lambda_t^{ij}(u_t, v_t)$  represent the function value of  $\lambda^{ij}$  at  $(u_t, v_t)$ , which is the centroid position of the tessellated triangle  $t$  in the parameter domain.  $\omega_t(\eta)$  is the signed solid angle of  $t$  toward  $\eta$ , which can be calculated by a general formulation Van Oosterom and Strackee [1983].

The coordinates of the Neumann term  $\psi_{Q_k}^{ij}(\eta)$  can be approximated calculated as:

$$\begin{aligned} \psi_{Q_k}^{ij}(\eta) &= \sum_t \iint_{(u,v) \in t} \frac{\lambda_t^{ij}(u,v)}{4\pi \|\mathbf{b}_t(u,v) - \eta\|} dvdu \\ &= \sum_t \iint_{(u,v) \in t} \frac{\lambda_t^{ij}(u,v)}{\|\mathbf{N}_t(u,v)\|} \overbrace{\frac{G(\xi, \eta) d\xi}{4\pi \|\mathbf{b}_t(u,v) - \eta\|}}^{G(\xi, \eta) d\xi} dvdu \\ &\approx \sum_t \frac{\lambda_t^{ij}(u_t, v_t)}{\|\mathbf{N}_t(u_t, v_t)\|} \int_{\xi \in t} G(\xi, \eta) d\xi, \end{aligned} \quad (28)$$

where  $\lambda_t^{ij}(u_t, v_t)$  denotes the function value of  $\lambda^{ij}$  at  $(u_t, v_t)$ , and  $\mathbf{N}_t(u_t, v_t)$  represents the surface normal at  $(u_t, v_t)$ . The expression  $\int_{\xi \in t} G(\xi, \eta) d\xi$  computes the integral of the fundamental solution of the 3D Laplacian equation over a planar triangle. This integral has a closed-form solution, and we directly apply the formulation given in the appendix of [Ben-Chen et al., 2009]. Additionally, we incorporate the correction factor for  $s(\xi)$  proposed by Thiery and Boubekeur [2022], which helps to reduce the issue of the deformed object extending beyond its boundaries in Green coordinates.

### 4.3 Linear reproduction

In previous section, we approximate the coordinates using Riemann summation. Additionally, we employ  $\mathbf{N}(u, v)$  of Eq. (14) to approximate  $(\mathbf{b}_u \times \mathbf{b}_v)(u, v)$  in Green's third identity. As a result, the linear reproduction property (Eq. (1)) will not completely hold. Although the approximation error may not be visually noticeable in the global appearance of deformed objects, the theoretical value of this section is important, as results that fail to satisfy linear reproduction typically do not conform to the conventional theoretical definition of coordinates. We observe that Thiery and Boubekeur [2022] introduce a per-quad projection approach for this topic. However, this method requires precomputing a tessellated cage and projecting the coordinates of each quad onto the summation results of tessellated triangles. We believe that approximating the curved surface with piecewise-linear triangles is not an optimal solution. In this work, we propose a global projection method to address this issue.

In Eq. (27) and (28), the approximated coordinates are derived and are now denoted as  $\bar{\phi}_{Q_k}^{ij}(\eta)$  and  $\bar{\psi}_{Q_k}^{ij}(\eta)$ , respectively. Here, a new index  $k$  is introduced to enumerate the Bézier patches. To ensure accurate linear reproduction, the modified coordinates  $\bar{\phi}_{Q_k}^{ij}(\eta)$  and  $\bar{\psi}_{Q_k}^{ij}(\eta)$  should satisfy the following equation precisely:

$$\eta = \sum_{k=1}^K \sum_{i=0}^m \sum_{j=0}^n (\bar{\phi}_{Q_k}^{ij}(\eta) \mathbf{b}_{ij}^{Q_k} + \bar{\psi}_{Q_k}^{ij}(\eta) \mathbf{N}_{ij}^{Q_k}), \quad (29)$$

which forms a linear system

$$\mathbf{A}\Phi = \eta, \quad (30)$$

where

$$\mathbf{A} = (\mathbf{b}_{00}^{Q_1}, \dots, \mathbf{b}_{mn}^{Q_1}, \mathbf{N}_{00}^{Q_1}, \dots, \mathbf{N}_{mn}^{Q_1}, \mathbf{b}_{00}^{Q_2}, \dots, \mathbf{N}_{mn}^{Q_K}) \in \mathbb{R}^{3 \times (2K(m+1)(n+1))}, \quad (31)$$

$$\Phi = (\bar{\phi}_{Q_1}^{00}(\eta), \dots, \bar{\phi}_{Q_1}^{mn}(\eta), \bar{\psi}_{Q_1}^{00}(\eta), \dots, \bar{\psi}_{Q_K}^{mn}(\eta))^T \in \mathbb{R}^{2K(m+1)(n+1)}. \quad (32)$$

We can assert that  $\mathbf{A}$  is always of rank 3, because we can find three control points that are not coplanar on the entire Bézier cage (typically a closed 2-manifold). These three columns of  $\mathbf{A}$  are linear independent. Given that  $\mathbf{A}$  has only three rows, and considering that the row rank of  $\mathbf{A}$  is equal to its column rank, we have  $\text{rank}(\mathbf{A}) = 3$ . Then, we can project  $\bar{\phi}_{Q_k}^{ij}(\eta)$  and  $\bar{\psi}_{Q_k}^{ij}(\eta)$  onto the solution space of Eq. (30). Specifically, we denote

$$\bar{\Phi} = (\bar{\phi}_{Q_1}^{00}(\eta), \dots, \bar{\phi}_{Q_1}^{mn}(\eta), \bar{\psi}_{Q_1}^{00}(\eta), \dots, \bar{\psi}_{Q_K}^{mn}(\eta))^T, \quad (33)$$

and formulate the optimization problem as:

$$\begin{aligned} \text{argmin}_{\Phi} \|\Phi - \bar{\Phi}\|_2, \\ \text{s.t. } \mathbf{A}\Phi = \eta. \end{aligned} \quad (34)$$

Let  $\mathbf{u} = \Phi - \bar{\Phi}$ , the problem is equivalent to finding the minimal-norm solution to  $\mathbf{A}\mathbf{u} = \eta - \mathbf{A}\bar{\Phi}$ , which has the solution  $\mathbf{u} = \mathbf{A}^+(\eta - \mathbf{A}\bar{\Phi})$ , where  $\mathbf{A}^+$  is the Moore-Penrose pseudoinverse of  $\mathbf{A}$ . Given that  $\mathbf{A}$  has full row rank, its pseudoinverse can be expressed as  $\mathbf{A}^+ = \mathbf{A}^T(\mathbf{A}\mathbf{A}^T)^{-1}$ . Since  $\mathbf{A}\mathbf{A}^T$  is a  $3 \times 3$  matrix, computing its inverse is computationally efficient. The expression for  $\Phi$  that achieves linear reproduction is:

$$\Phi = \bar{\Phi} + \mathbf{A}^T(\mathbf{A}\mathbf{A}^T)^{-1}(\eta - \mathbf{A}\bar{\Phi}). \quad (35)$$

The most direct way to verify linear reproduction is to check if the output model matches the input model exactly when the source and target cages are identical. Fig. 3 (a) and (b) respectively illustrate the results without and with the global projection approach. The color bar indicates that the Riemann summation introduces typical errors, whereas the global projection method achieves perfect linear reproduction.

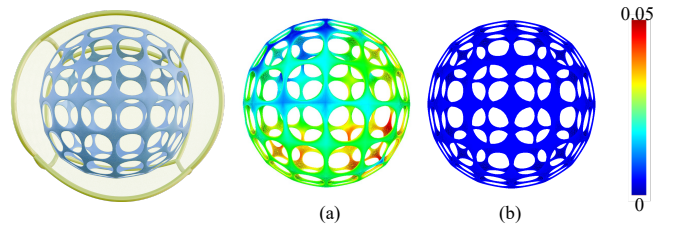


Figure 3: Results without (a) and with (b) global projection approach. Our method perfectly achieves linear reproduction.

### 4.4 Discussion

In this section, we will explore the primary advantages of establishing Green coordinates for Bézier cages. A key benefit is that our method enables effective control over shape deformation. We observe that a recent work [Qin et al., 2024] proposes  $C^0$

generalized Coons patches for cage-based deformation. Our method differs from this approach in the following aspects: 1) In current 3D implementation,  $C^0$  GC patch is mainly controlled by 3D curves instead of a complete closed surface cage. 2)  $C^0$  GC patch does not account for scenarios where the source cage is curved, as it only considers cases where the target cage is curved. This limitation restricts its ability to design a more compact source cage. 3)  $C^0$  GC patch primarily establishes generalized barycentric coordinates. While these coordinates are more consistent with the cage shape, the resulting deformations may exhibit shearing artifacts and appear less natural compared to the original shape. In contrast, our method incorporates normal information and establishes Green coordinates with normal controls, which exhibit enhanced shape preservation properties, as demonstrated in Fig. 4.

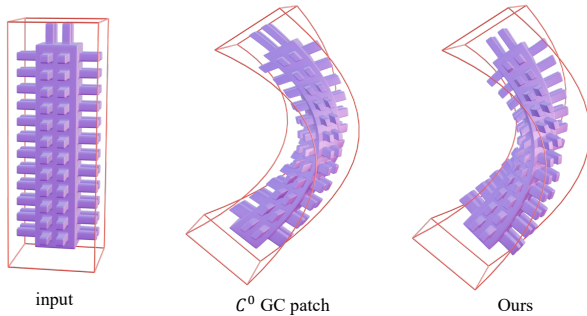


Figure 4: Our approach demonstrates superior shape preservation properties compared to  $C^0$  GC patch [Qin et al., 2024].

A degree- $(m, n)$  tensor product Bézier patch consists of  $2(m + n)$  boundary control points and  $(m + 1)(n + 1) - 2(m + n)$  interior control points. Some may be concerned that directly designing the interior control points for Bézier patches can be challenging. However, by leveraging the fact that the tensor product operation commutes with Coons operations Farin [1992b], we can directly obtain the interior control points of the bilinear blended patch from the boundary Bézier curves and construct a complete Bézier control net. This process is detailed in Appendix B. As a result, our approach does not complicate the cage design compared to  $C^0$  GC patch.

## 5 Experiments

### 5.1 Overview

In this section, we present the results of our method and conduct a comparative analysis with related approaches. To the best of our knowledge, our approach is the first to construct Green coordinates for 3D Bézier cages. Additionally, we did not find any publicly available Bézier cage models in previous methods. To obtain valid data for testing our algorithm, we start by modifying the quad cage provided by Thiery et al. [2018]. Each quad  $\mathbf{q}(u, v)$  is then expanded into a degree- $(3, 3)$  Bézier patch by introducing additional control points at positions  $\mathbf{q}(\frac{i}{3}, \frac{j}{3})$  where  $i, j \in \{0, 1, 2, 3\}$ . We subsequently design new positions for the Bézier control points, enabling the generation of compact source cage for original shapes. The design process

is completed with the help of Blender and its Python script. Subsequently, we create the target cage by adjusting Bézier control points based on requirements, and conduct deformation using Green coordinates established on the Bézier cage. A well-designed and tightly constructed initial cage ensures that the deformed result aligns more closely with the target cage. This phenomenon is illustrated in Fig. 5, where the tighter cage (b) yields superior results, as evidenced by the handle of the vase.

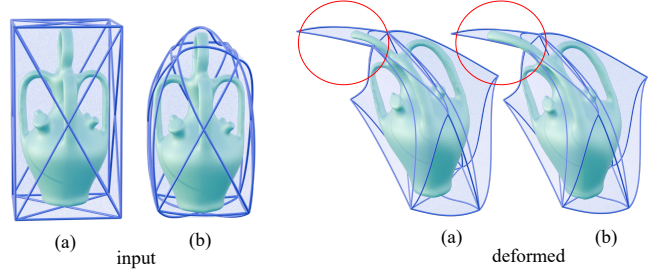


Figure 5: Deformation results of different source cages. The tighter cage (b) yields better results.

### 5.2 Comparisons

In this section, we compare our method with related approaches, including: 1) Green coordinates of triangle cages (denoted as GC hereafter) Lipman et al. [2008]; 2) Mean value coordinates of quad cages (denoted as QMVC hereafter) Thiery et al. [2018]; and 3) Green coordinates of quad cages (denoted as QGC hereafter) Thiery and Boubekeur [2022]. We use the implementation provided by Ströter et al. [2024] for all comparative analyses. Given that quads are limited to representing straight boundaries, it is evident that using a single quad to approximate a Bézier patch would not yield good results. To make a more compelling comparison, we generate tessellated quad cages for QMVC and QGC by subdividing each degree- $(3, 3)$  Bézier patch into 9 quads along the  $u$  and  $v$  directions. Specifically, for a Bézier patch  $\mathbf{b}(u, v)$ , we introduce quad vertices at  $\mathbf{b}(\frac{i}{3}, \frac{j}{3})$  for  $i, j \in \{0, 1, 2, 3\}$ , thereby subdividing the patch into 9 quads. Fig. 6 (a) shows a typical bar model for comparison. We can observe that QMVC and QGC produces segmented structures. In Fig. 6 (b), we compare our method with GC, where each Bézier patch is divided into  $3 \times 3 \times 2$ ,  $4 \times 4 \times 2$ , or  $10 \times 10 \times 2$  triangles. It is evident that using fewer triangles still results in segmented outcomes. Although increasing the number of triangles allows for a better approximation of curved edges, it necessitates the storage of a large number of coordinates. Given that these coordinates are computed only once and do not need to be recalculated for new deformations of the same model, employing a tessellated cage would increase the time required for each deformation.

Fig. 7 presents additional comparisons with GC, QMVC, QGC, where each Bézier patch is divided into 9 quads or 18 triangles. We can observe that: 1) While QMVC aligns more closely with the cage, it may introduce shearing artifacts and produce less natural outputs. In contrast, Green coordinates demonstrate superior shape-preserving properties. 2) Employing Bézier cages

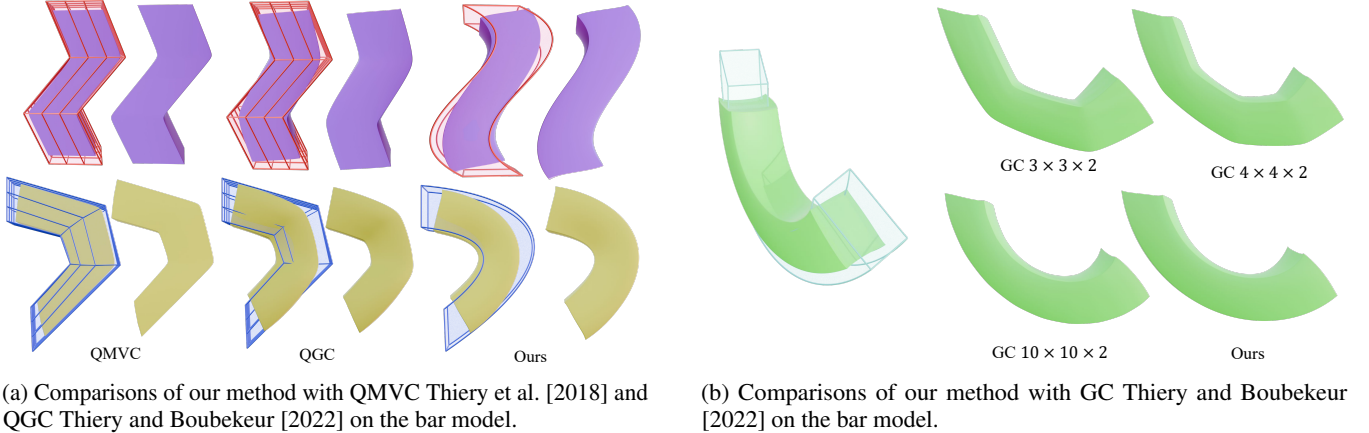


Figure 6: Comparisons of our method with different methods on the bar model.

Table 1: Running time of different approaches (in seconds).

Model/Method	$V$	$B$	GC-18	QMVC-9	QGC-9	Ours
Cactus	98820	34	5.00	102.89	124.62	27.80
Bench	65430	22	2.16	42.30	51.42	11.79
Bar	229378	6	2.12	41.57	49.99	8.54
FireHydrant	39028	46	2.67	54.79	67.04	14.73
WireSphere	48964	6	0.45	8.78	10.66	2.54

results in better performance for bending and high-curvature deformations. When the cage is subdivided into multiple quads or triangles, it becomes evident that the deformed object exhibits segmented structures. Additionally, designing the subdivided quad cage does not appear to be easier than designing the Bézier cage.

Fig. 8 demonstrates the deformation results of our method applied to cages constructed by Bézier triangles (top row) and tensor product Bézier patches (bottom two rows), highlighting the broad applicability of our approach.

### 5.3 Running times

Tables 1 presents the running time of different approaches. The running time of our method includes the global projection method described in Section 4.3. All experiments are conducted on a standard laptop equipped with a 10-core Intel CPU at 2.40 GHz with 16GB RAM. The implementations are carried out in C++ along with Eigen libraries [Guennebaud et al., 2025] on Windows.

In the table,  $V$  and  $B$  represent the number of mesh vertices and the number of Bézier cage patches, respectively. QGC-9 and QMVC-9 report the time taken by QMVC and QGC after subdividing each Bézier patch into 9 quads. Given that all quads require domain tessellation, QMVC-9 and QGC-9 requires considerable computational time. GC-18 reports the time taken by GC after subdividing each Bézier patch into 18 triangles. Since GC has a closed-form solution, GC-18 is computationally efficient; however, it produces segmented shapes for high-curvature deformations. Subdividing the Bézier patch into denser triangles can better approximate the original curved

cage. However, this requires storing a larger set of vertex coordinates. Given that once the coordinates are precomputed, they do not need to be recalculated for subsequent deformations, this approach may increase the computation time for each deformation.

## 6 Conclusion

In this work, we introduce a cage-based deformation method that constructs Green Coordinates on Bézier patches, allowing for the design of tightly fitted cages and enabling flexible deformation of curved shapes. The coordinates are established on the positions and normals of the Bézier control net. Additionally, we propose a global solution space projection method to ensure linear reproduction of the coordinates. Experimental results demonstrate that our method achieves smooth boundaries for high curvature deformations.

Our approach still has limitations. Firstly, the coordinates do not have a closed-form solution. Although we provide a method to ensure linear reproduction, the Riemann summation incurs a certain amount of computational time. Additionally, while Green coordinates enable shape-preserving deformations, we cannot guarantee that the deformed shape will remain entirely within the cage. In future work, we will continue to explore new ideas regarding high-order cages.

## A Green coordinates on Bézier triangles

This section will detail the establishment of Green coordinates on Bézier triangles, a widely-used data structure for representing higher-order surfaces. A degree- $n$  Bézier triangle is defined by two parameters  $u$  and  $v$ , subject to the constraints  $0 \leq u \leq 1$ ,  $0 \leq v \leq 1$ , and  $0 \leq u + v \leq 1$ . The parametric equation of the Bézier triangle can be expressed as:

$$\mathbf{b}(u, v) = \sum_{\substack{i+j+k=n \\ i,j,k \geq 0}} \frac{n!}{i!j!k!} u^i v^j (1-u-v)^k \mathbf{b}_{ijk}. \quad (36)$$



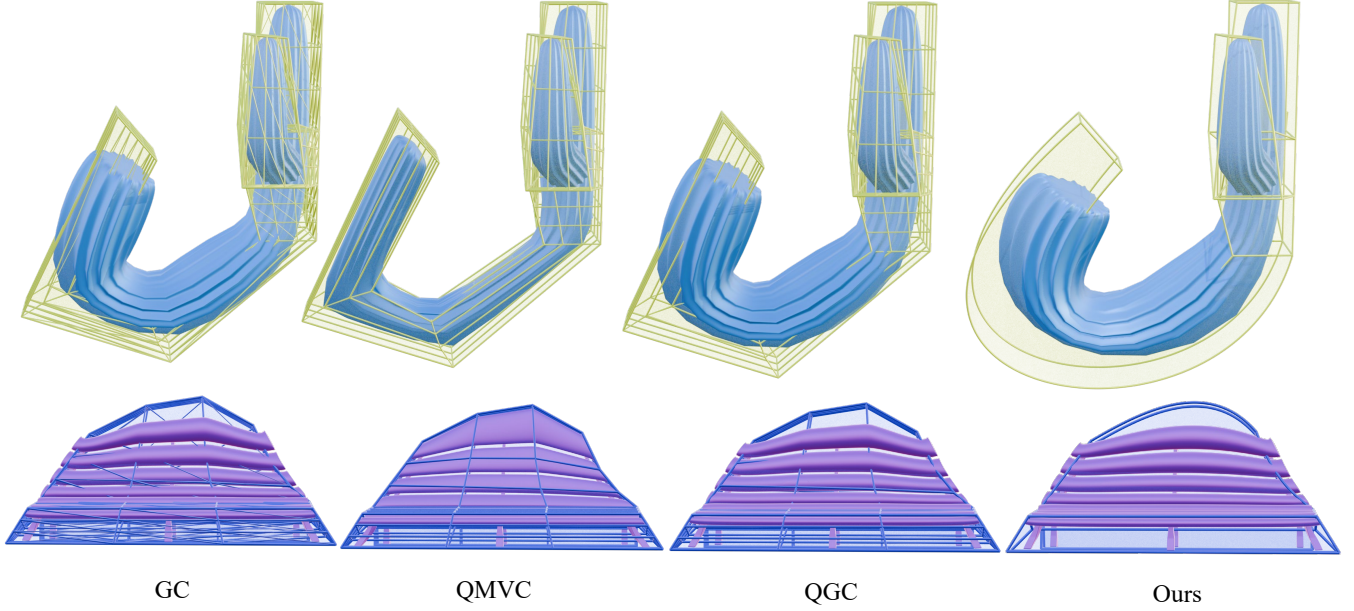


Figure 7: Comparisons of our method with GC [Lipman et al., 2008], QMVC Thiery et al. [2018] and QGC Thiery and Boubekeur [2022].

We can denote  $\gamma^{ijk}(u, v) = \frac{n!}{i!j!k!}u^i v^j (1-u-v)^k$  and express the Bézier triangle as:

$$\mathbf{b}(u, v) = \sum_{\substack{i+j+k=n \\ i,j,k \geq 0}} \gamma^{ijk}(u, v) \mathbf{b}_{ijk}. \quad (37)$$

Similar to tensor product Bézier patches, we also establish Green coordinates for Bézier triangles based on the vertices and unnormalized normals of their control nets. Initially, vertex normals are constructed for each control point, and subsequently, the normals for arbitrary  $(u, v)$  on the surface are computed using the parametric equations. The normals  $\mathbf{N}_{ijk}$  of control vertex  $\mathbf{b}_{ijk}$  is constructed by the cross product of its one-ring neighbour. For instance,  $\mathbf{N}_{ijk}$  in Fig. 9 is constructed by:

$$\begin{aligned} \mathbf{N}_{ijk} = \frac{n^2}{6} [ & (\mathbf{b}_{(i+1)j(k-1)} - \mathbf{b}_{ijk}) \times (\mathbf{b}_{i(j+1)(k-1)} - \mathbf{b}_{ijk}) \\ & + (\mathbf{b}_{i(j+1)(k-1)} - \mathbf{b}_{ijk}) \times (\mathbf{b}_{(i-1)(j+1)k} - \mathbf{b}_{ijk}) \\ & + (\mathbf{b}_{(i-1)(j+1)k} - \mathbf{b}_{ijk}) \times (\mathbf{b}_{(i-1)j(k+1)} - \mathbf{b}_{ijk}) \\ & + (\mathbf{b}_{(i-1)j(k+1)} - \mathbf{b}_{ijk}) \times (\mathbf{b}_{i(j-1)(k+1)} - \mathbf{b}_{ijk}) \\ & + (\mathbf{b}_{i(j-1)(k+1)} - \mathbf{b}_{ijk}) \times (\mathbf{b}_{(i+1)(j-1)k} - \mathbf{b}_{ijk}) \\ & + (\mathbf{b}_{(i+1)(j-1)k} - \mathbf{b}_{ijk}) \times (\mathbf{b}_{(i+1)j(k-1)} - \mathbf{b}_{ijk}) ]. \end{aligned} \quad (38)$$

Then, the surface normal  $\mathbf{N}(u, v)$  for parameter  $(u, v)$  inside the Bézier triangle is calculated as:

$$\mathbf{N}(u, v) = \sum_{\substack{i+j+k=3 \\ i,j,k \geq 0}} \gamma^{ijk}(u, v) \mathbf{N}_{ijk}. \quad (39)$$

$\mathbf{N}(u, v)$  is linear with respect to  $\mathbf{N}_{ijk}$ , allowing us to construct the Neumann term of the Green coordinates. By applying a

similar calculation method as described in Section 4 of the main text, the deformed position  $\tilde{\eta}$  can be expressed as:

$$\tilde{\eta} = \sum_T (\tilde{f}_D^T(\eta) + \tilde{f}_N^T(\eta)) = \sum_T \sum_{\substack{i+j+k=n \\ i,j,k \geq 0}} (\phi_T^{ijk}(\eta) \tilde{\mathbf{b}}_{ijk}^T + \psi_T^{ijk}(\eta) \tilde{\mathbf{N}}_{ijk}^T), \quad (40)$$

where

$$\phi_T^{ijk}(\eta) = \int_{u=0}^1 \int_{v=0}^{1-u} \frac{\gamma_T^{ijk}(u, v) (\mathbf{b}_T(u, v) - \eta) \cdot \mathbf{N}_T(u, v)}{4\pi \|\mathbf{b}_T(u, v) - \eta\|^3} dv du, \quad (41)$$

$$\psi_T^{ijk}(\eta) = \int_{u=0}^1 \int_{v=0}^{1-u} \frac{\gamma_T^{ijk}(u, v)}{4\pi \|\mathbf{b}_T(u, v) - \eta\|} dv du. \quad (42)$$

Here,  $T$  represent one Bézier triangle,  $\tilde{\mathbf{b}}_{ijk}^T$  and  $\tilde{\mathbf{N}}_{ijk}^T$  denote the positions and normals of the control vertices in the deformed cage, respectively.

Experimental results for Bézier triangle cages are presented in the right example of Fig. 1 and the first row of Fig. 8 in the main text.

## B Generating bilinear blended interior vertices

In Section 4.4, we compare our method with  $C^0$  GC patch Qin et al. [2024] and highlight the advantage of constructing coordinates on the entire Bézier patch rather than 3D curves. Some may be concerned that directly designing interior control points for Bézier patches is quite difficult. This section mainly explains that this concern is not that necessary, as initial interior control vertices for bilinear blending patches can be easily generated when boundary curves are provided.

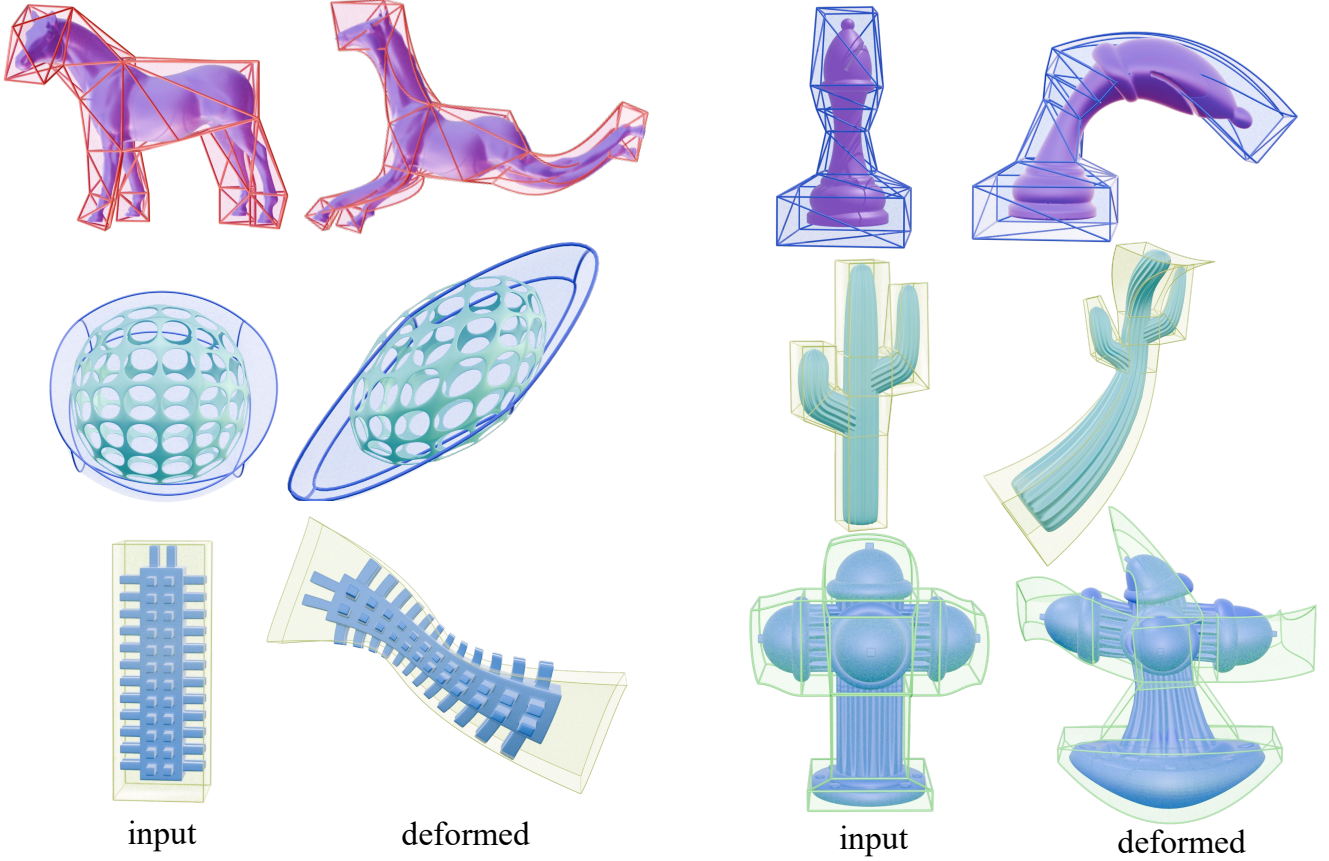


Figure 8: Deformation results of our method in cages constructed by Bézier triangles (top row) and tensor product Bézier patches (bottom two rows).

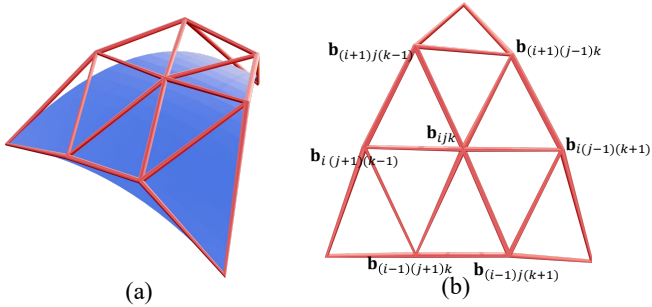


Figure 9: Illustration of a Bézier triangle patch (a) and its control net (b).

Given four boundary curves, it is possible to interpolate a surface that passes through these boundaries, a concept commonly referred to as the Coons patch problem Coons [1967]. The simplest approach is bilinear blending. Considering four boundary curves that are sequentially connected, denoted as  $s(0, v)$ ,  $s(1, v)$ ,  $s(u, 0)$ ,  $s(u, 1)$ , the Coon patch  $Cs(u, v)$  can

be interpolated as:

$$Cs(u, v) = (1 - u)s(0, v) + us(1, v) + (1 - v)s(u, 0) + vs(u, 1) - (1 - u, u) \begin{pmatrix} s(0, 0) & s(0, 1) \\ s(1, 0) & s(1, 1) \end{pmatrix} \begin{pmatrix} 1 - v \\ v \end{pmatrix}. \quad (43)$$

We can verify that  $Cs(u, v)$  is a parametric surface that indeed interpolates the four given boundary curves. However,

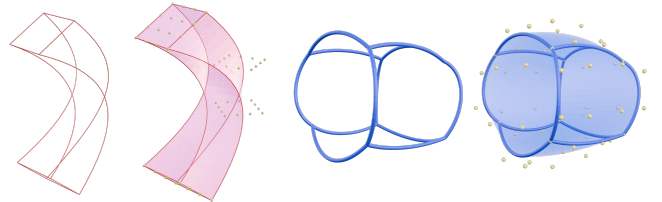


Figure 10: Given the boundary Bézier curves, we can generate the control points (yellow points) of the bilinear blended Bézier cage.

directly applying the Coons patch formulation to boundary curves presents a challenge in constructing Green coordinates due to the lack of interior control points, which are necessary for

the construction of vertex normals. Fortunately, Farin [1992b] notes that the tensor product operation commutes with Coons operations. Therefore, instead of using the Bézier curve formulation for  $s$  as given in Eq. (43), we define  $s(0, v)$ ,  $s(1, v)$ ,  $s(u, 0)$ ,  $s(u, 1)$  as the four piecewise linear functions corresponding to the control net along the four boundary Bézier curves. Then, we position the interior control points  $\mathbf{b}_{ij}$  at

$$\mathbf{b}_{ij} = Cs\left(\frac{i}{m}, \frac{j}{n}\right), \quad (44)$$

where  $i = \{1, 2, \dots, m-1\}$ ,  $j = \{1, 2, \dots, n-1\}$ . This process generates all the control points for the entire Bézier control net of the bilinear blended surface. Fig. 10 illustrates several examples where we generate the control points of the bilinear blended Bézier cage using only the boundary Bézier curves. The interior control points can be further adjusted as needed by the user.

Additionally, Bézier triangles also possess a Coons patch formulation, which is illustrated in Section 21.6 of Farin [1992a].

## References

- Mirela Ben-Chen, Ofir Weber, and Craig Gotsman. Variational harmonic maps for space deformation. *ACM Transactions on Graphics*, 28(3):34, 2009.
- Tao Ju, Scott Schaefer, and Joe D. Warren. Mean value coordinates for closed triangular meshes. *ACM Transactions on Graphics*, 24(3):561–566, 2005.
- Jean-Marc Thiery, Pooran Memari, and Tamy Boubekeur. Mean value coordinates for quad cages in 3D. *ACM Transactions on Graphics*, 37(6):229, 2018.
- Pushkar Joshi, Mark Meyer, Tony DeRose, Brian Green, and Tom Sanocki. Harmonic coordinates for character articulation. *ACM Transactions on Graphics*, 26(3):71, 2007.
- Xian-Ying Li and Shi-Min Hu. Poisson coordinates. *IEEE Transactions on Visualization and Computer Graphics*, 19(2):344–352, 2013.
- Yaron Lipman, David Levin, and Daniel Cohen-Or. Green coordinates. *ACM Transactions on Graphics*, 27(3):78, 2008.
- Jean-Marc Thiery and Tamy Boubekeur. Green coordinates for triquad cages in 3D. In *SIGGRAPH Asia 2022 Conference Papers*, pages 38:1–38:8. ACM, 2022.
- Élie Michel and Jean-Marc Thiery. Polynomial 2D Green coordinates for polygonal cages. In *ACM SIGGRAPH 2023 Conference Proceedings*, pages 23:1–23:9. ACM, 2023.
- Jason Smith and Scott Schaefer. Selective degree elevation for multi-sided Bézier patches. *Computer Graphics Forum*, 34(2):609–615, 2015.
- Kaikai Qin, Yunhao Zhou, Chenhao Ying, Yajuan Li, and Chongyang Deng.  $c^0$  generalized coons patches for high-order cage-based deformation. *ACM Transactions on Graphics*, 43(6), 2024.
- Michael S. Floater. Generalized barycentric coordinates and applications. *Acta Numerica*, 24:161–214, 2015.
- Kai Hormann and Narayan Sukumar. *Generalized barycentric coordinates in computer graphics and computational mechanics*. CRC Press, Boca Raton, FL, 1st edition, 2017.
- Daniel Ströter, Jean-Marc Thiery, Kai Hormann, Jiong Chen, Qingjun Chang, Sebastian Besler, Johannes Mueller-Roemer, Tamy Boubekeur, André Stork, and Dieter W. Fellner. A survey on cage-based deformation of 3D models. *Computer Graphics Forum*, 43(2):i–iii, 2024.
- Zhipei Yan and Scott Schaefer. A family of barycentric coordinates for co-dimension 1 manifolds with simplicial facets. *Computer Graphics Forum*, 38(5):75–83, 2019.
- Ana Dodik, Oded Stein, Vincent Sitzmann, and Justin Solomon. Variational barycentric coordinates. *ACM Transactions on Graphics*, 42(6):255:1–255:16, 2023.
- Michael S. Floater. Mean value coordinates. *Computer Aided Geometric Design*, 20(1):19–27, 2003.
- Michael S. Floater, Géza Kós, and Martin Reimers. Mean value coordinates in 3D. *Computer Aided Geometric Design*, 22(7):623–631, 2005.
- Torsten Langer, Alexander G. Belyaev, and Hans-Peter Seidel. Spherical barycentric coordinates. In *Proceedings of the Fourth Eurographics Symposium on Geometry Processing*, volume 256, pages 81–88. Eurographics Association, 2006.
- Yaron Lipman, Johannes Kopf, Daniel Cohen-Or, and David Levin. Gpu-assisted positive mean value coordinates for mesh deformations. In *Proceedings of the Fifth Eurographics Symposium on Geometry Processing*, volume 257, pages 117–123. Eurographics Association, 2007.
- Xian-Ying Li, Tao Ju, and Shi-Min Hu. Cubic mean value coordinates. *ACM Transactions on Graphics*, 32(4):126:1–126:10, 2013.
- Kai Hormann and N. Sukumar. Maximum entropy coordinates for arbitrary polytopes. *Computer Graphics Forum*, 27(5):1513–1520, 2008.
- Qingjun Chang, Chongyang Deng, and Kai Hormann. Maximum likelihood coordinates. *Computer Graphics Forum*, 42(5):i–viii, 2023.
- Yaron Lipman and David Levin. Derivation and analysis of Green coordinates. *Computational Methods and Function Theory*, 10(1):167, 2009.
- Shibo Liu, Ligang Liu, and Xiao-Ming Fu. Polynomial 2d Green coordinates for high-order cages. *CoRR*, abs/2408.06831, 2024a. URL <https://doi.org/10.48550/arXiv.2408.06831>.
- Ofir Weber, Roi Poranne, and Craig Gotsman. Biharmonic coordinates. *Computer Graphics Forum*, 31(8):2409–2422, 2012.
- Jean-Marc Thiery, Élie Michel, and Jiong Chen. Biharmonic coordinates and their derivatives for triangular 3D cages. *ACM Transactions on Graphics*, 43(4):138:1–138:17, 2024.
- Jiong Chen, Fernando de Goes, and Mathieu Desbrun. Somigliana coordinates: an elasticity-derived approach for cage deformation. In *ACM SIGGRAPH 2023 Conference Proceedings*, pages 52:1–52:8. ACM, 2023.

- Ofir Weber, Mirela Ben-Chen, and Craig Gotsman. Complex barycentric coordinates with applications to planar shape deformation. *Computer Graphics Forum*, 28(2):587–597, 2009.
- Zhehui Lin and Renjie Chen. Polynomial cauchy coordinates for curved cages. In *SIGGRAPH Asia 2024 Conference Papers*, pages 67:1–67:8. ACM, 2024.
- Gerald E. Farin. *Curves and surfaces for computer aided geometric design - a practical guide, 3rd Edition*. Computer science and scientific computing. Academic Press, 1992a. ISBN 978-0-12-249052-1.
- Yixin Hu, Teseo Schneider, Xifeng Gao, Qingnan Zhou, Alec Jacobson, Denis Zorin, and Daniele Panozzo. Triwild: robust triangulation with curve constraints. *ACM Transactions on Graphics*, 38(4):52:1–52:15, 2019.
- Manish Mandad and Marcel Campen. Bézier guarding: precise higher-order meshing of curved 2d domains. *ACM Transactions on Graphics*, 39(4):103, 2020.
- Jinlin Yang, Shibo Liu, Shuangming Chai, Ligang Liu, and Xiao-Ming Fu. Precise high-order meshing of 2D domains with rational Bézier curves. *Computer Graphics Forum*, 41(5):79–88, 2022.
- Zhongshi Jiang, Ziyi Zhang, Yixin Hu, Teseo Schneider, Denis Zorin, and Daniele Panozzo. Bijective and coarse high-order tetrahedral meshes. *ACM Transactions on Graphics*, 40(4):157:1–157:16, 2021.
- Shibo Liu, Yang Ji, Jia-Peng Guo, Ligang Liu, and Xiao-Ming Fu. Smooth bijective projection in a high-order shell. *ACM Transactions on Graphics*, 43(4):59:1–59:13, 2024b.
- Alex Vlachos, Jörg Peters, Chas Boyd, and Jason L. Mitchell. Curved PN triangles. In *Proceedings of the 2001 Symposium on Interactive 3D Graphics*, pages 159–166. ACM, 2001.
- Steven J. Owen, David R. White, and Timothy J. Tautges. Facet-based surfaces for 3D mesh generation. In *International Meshing Roundtable Conference*, 2002.
- Shi-Min Hu and Johannes Wallner. A second order algorithm for orthogonal projection onto curves and surfaces. *Computer Aided Geometric Design*, 22:251–260, 2005.
- A. Van Oosterom and J. Strackee. The solid angle of a plane triangle. *IEEE Transactions on Biomedical Engineering*, BME-30(2):125–126, 1983.
- Gerald E. Farin. Commutativity of coons and tensor product operators. *Rocky Mountain Journal of Mathematics*, 22:541–546, 1992b.
- Gaël Guennebaud, Benoît Jacob, et al. Eigen v3. <http://eigen.tuxfamily.org>, 2025. Accessed: 2025-1-23.
- S.A. Coons. Surfaces for computer-aided design of space forms. Technical Report MIT/LCS/TR-41, Massachusetts Institute of Technology, Cambridge, MA, June 1967. Published as a Technical Report by the Laboratory for Computer Science.